# Three-Dimensional Percolation and Performance of Nanocrystal Field-Effect Transistors

Willi Aigner,[1] Markus Wiesinger,[1] Hartmut Wiggers,[2] Martin Stutzmann,[1] and Rui N. Pereira[1,3,*]

[1]*Walter Schottky Institut and Physik-Department, Technische Universität München, Am Coulombwall 4, 85748 Garching, Germany*

[2]*Institute for Combustion and Gasdynamics-Reactive Fluids-and CENIDE, Center for Nanointegration Duisburg-Essen, Universität Duisburg-Essen, Carl-Benz-Straße 199, 47057 Duisburg, Germany*

[3]*Department of Physics and I3N, University of Aveiro, 3810-193 Aveiro, Portugal*

(Received 18 November 2015; revised manuscript received 2 March 2016; published 24 May 2016)

The understanding of charge transport through films of semiconductor nanocrystals (NCs) is fundamental for most applications envisaged for these materials, e.g., light-emitting diodes, solar cells, and thin-film field-effect transistors (FETs). In this work, we show that three-dimensional film-thickness-dependent percolation effects taking place above the percolation threshold strongly affect the charge transport in NC films and greatly determine the performance of NC devices such as NC FETs. We use thin films of Si NCs with a wide range of thicknesses controllable by spray coating of NC inks to thoroughly investigate the electronic properties and charge transport in thin NC films. We find a steep (superlinear) increase of the electrical conductivity with increasing film thickness, which is not observed in bulk semiconductor thin films with bandlike charge transport. We explain this increase by an exponentially increasing number of charge percolation paths in a system dominated by hopping charge transport. Thin-film NC FETs reveal thickness-independent field-effect mobilities and threshold voltages, whereas on:off current ratios decrease quickly with increasing film thickness. We show that the steep enhancement of electrical conductivity with increasing film thickness provided by three-dimensional percolation effects is, in fact, responsible for the dramatic degradation of NC FET performance observed with increasing film thickness. Our work demonstrates that the performance of NC FETs is much more critically sensitive to film thickness than in conventional FET-based bulk semiconductor materials.

DOI: 10.1103/PhysRevApplied.5.054017

## I. INTRODUCTION

Thin films of semiconductor nanocrystals (NCs) have been investigated for their use in new technologies taking advantage of the unique optical and electronic properties of NCs [1–7]. Liquid dispersions of NCs (NC inks) are particularly attractive from the perspective of processing since thin films can be easily printed, spin cast, or spray cast on large areas of patterned substrates in contrast to expensive vacuum-deposition techniques [8–10]. The application of thin films of NCs in many (opto)electronic devices including solar cells, light-emitting diodes, and field-effect transistors (FETs) is currently under investigation [6,11–16]. NC FETs are devices commonly applied also for evaluating the electronic properties of NC films, as FETs can be used to measure electronic transport characteristics such as electrical conductivity and field-effect charge carrier mobility. NC FETs have been reported using Cd*X* and Pb*X* ($X =$ S, Se, Te) NCs [5,17–24], Si NCs, and Ge NCs [8,9,25–29]. Cd*X* and Pb*X* NC FETs typically exhibit superior electronic properties with (ambipolar) field-effect mobilities already approaching those observed in organic semiconductors [6], whereas the development of FETs made of Si and Ge NCs is still lagging behind. On the track to making NC FETs competitive with respect to current inorganic semiconductor thin-film technology, a deeper understanding of the charge-transport mechanisms is required. For Si NC films, studies have reported hopping transport mechanisms, such as space-charge-limited current with an exponential distribution of trap states and Fowler-Nordheim tunneling [30–35]. For Pb*X* NC films, a possible more bandlike transport via delocalized states is under discussion [36,37]. In NC systems, charge percolation effects should significantly change the magnitude of the electrical conductivity, in particular, in systems exhibiting hopping transport via localized states. However, percolation effects in semiconductor NC systems have, so far, been studied only in conducting systems composed of NCs embedded in an insulating matrix [38]. Here, the volume fraction of the NCs in the system (film) has to be above the percolation threshold to create continuous macroscopic conducting paths between two electrodes [39]. In three dimensions (3D), systems above the percolation threshold are expected to show a strong dependence of the conductivity on the film thickness. This effect has been theoretically investigated by Shklovskii *et al.* [40–42] considering

*pereira@wsi.tum.de

 © 2016 American Physical Society

strongly inhomogeneous media. As far as NC systems are concerned, experimental results have been published by Müller *et al.* [43] reporting an exponential dependence of the conductivity of Au NCs on film thickness, presumably due to 3D percolation effects. In this work, we address the impact of 3D percolation effects on the charge transport of semiconductor NC films and devices such as NC FETs.

We investigate NC FETs made of Si NCs as a model system to study the charge-transport properties of NC thin films. In particular, the impact of percolation effects on NC FET performance is investigated systematically. NC FETs in the bottom-gate configuration are fabricated using spray-coating deposition enabling a controlled film thickness and homogeneous morphology, which we find to be key to achieving well-working NC FETs and study percolation effects via variation of the NC film thickness. Current-voltage measurements are performed to extract the electrical conductivity of the NC films, showing a space-charge-limited current behavior with a pronounced dependence on film thickness. Transistor characteristics and transfer curves are recorded to obtain the field-effect mobility, the threshold voltage, and the transistor performance (i.e., the on:off current ratio). Whereas the field-effect mobility and the threshold voltage do not show a significant dependence on the film thickness, the transistor on:off current ratio strongly decays with increasing film thickness, which is in contrast to conventional thin-film FETs. We can explain the rapid deterioration of the NC FETs performance with percolation effects, thus, making our study relevant for any semiconductor NC devices relying on charge transport through a 3D network of NCs.

## II. METHODS

### A. Si NC synthesis and ink preparation

Si NCs are synthesized by microwave-induced decomposition of silane in a low-pressure flow reactor [44]. The NC size is controlled by adjusting the gas flow rate of silane, Ar, and $H_2$. In this work, as-grown Si NCs with a mean diameter $d_{\text{as grown}} = 19$ nm, as determined by the Brunauer-Emmet-Teller method [45], are used. The as-grown Si NCs are covered with a thin amorphous oxide layer due to exposure to air, which is removed using HF wet etching rendering H-terminated Si NCs [34]. For this procedure, the as-grown Si NC powder is moistened with ethanol and mixed in excess with an aqueous HF solution (10% vol). After a 10-min reaction time, the suspension is mixed with chlorobenzene. As the HF-etched Si NCs (H-terminated) become hydrophobic, they transfer into the chlorobenzene, which is separated from the HF solution due to its different density. In a subsequent step, the HF aqueous solution is removed, and the Si NCs are precipitated from the chlorobenzene suspension by centrifuging (2 min at 4000 rpm). The precipitate is then mixed with a fixed volume of chlorobenzene to achieve a cloudy suspension ("ink") containing 1 wt % of H-terminated Si NCs in chlorobenzene. Fourier-transform infrared spectroscopy (FTIR) confirms that the Si NCs are H terminated after this process (see the Supplemental Material [46] and Refs. [47,48]). The size distribution of the H-terminated Si NCs is determined by high-magnification scanning electron microscopy (SEM) [see example in Fig. 1(a)], which is recorded using Si NC films with a Zeiss NVision 40 microscope. From the distribution of NC sizes shown in Fig. 1(b), we find a log-normal distribution with a count median diameter $d_{\text{H term}} = 10 \pm 2$ nm.

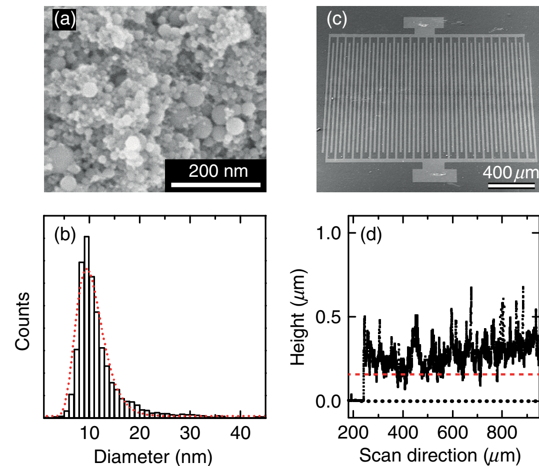


FIG. 1. (a) High-magnification SEM image of HF-etched Si NCs (H terminated). (b) Size distribution of Si NCs in (a). The red dotted line is a fit of a log-normal distribution with a count median diameter $d_{\text{H term}} = 10 \pm 2$ nm. (c) SEM image of a FET electrode structure covered with a thin Si NC film obtained under an angle of 60°. (d) Surface profile of the FET structure in (c).

### B. Si NC FET fabrication and characterization

Bottom-gate Si NC FETs are fabricated on highly *p*-type doped Si substrates covered with a 50-nm silicon nitride dielectric layer. Interdigit Au contact structures consisting of 50 fingers with a length of 1.88 mm, 20-$\mu$m spacing, and 130-nm thickness are patterned on top of the substrates using photolithography and thermal evaporation. The Si NCs are deposited on these substrates by means of a spray-coating technique with a well-defined volume of Si NC ink in a homemade system. To avoid reoxidation of the Si NCs, the film deposition is carried out under $N_2$ atmosphere. The spray-coating technique enables the deposition of homogeneous Si NC films with a thickness controlled by applying multiple spray cycles. This has not been possible using spin coating, which instead gives rise to the appearance of large agglomerates and uncovered areas (see the Supplemental Material [46]). Figure 1(c) shows a SEM image of a Si NC film under an angle of 60°. The film exhibits a smooth surface and has no large pinholes. In Fig. 1(d), a surface profile of the film in Fig. 1(c) is shown. Here, we use a DekTak 150 surface profiler with a stylus

diameter of 12.5 $\mu$m. As can be seen, the height of the films is roughly constant and has a considerable surface roughness of about 100–200 nm. We define the effective thickness of the films $L$ as the lower 5 percentile [red dashed line in Fig. 1(d)] where a continuous coverage over the whole sample is ensured. Electrical measurements are carried out in an Ar-purged glove box (oxygen and water concentration <1 ppm) in darkness and at room temperature. We use a homemade needle-station setup equipped with two Keithley 2400 source meter units to measure current ($I$) versus voltage ($V$) characteristics ($I$-$V$) with floating-gate, transistor-output characteristics with an applied gate voltage (drain-source current $I_{\mathrm{DS}}$ versus drain-source voltage $V_{\mathrm{DS}}$ as a function of gate voltage $V_G$), and transfer curves with a fixed drain-source voltage ($I_{\mathrm{DS}}$ versus $V_G$ with fixed $V_{\mathrm{DS}}$). The scan rate is chosen to be 1 V s$^{-1}$. We fabricate three independent sets of films with different thicknesses. In this way, we can investigate scattering and ensure reproducibility of the variations of the data with film thickness.

## III. EXPERIMENTAL DATA

### A. Current-voltage characteristics

In Fig. 2(a), typical $I$-$V$ characteristics (floating gate) are shown for NC films with different thicknesses. The data are chosen from the same set of samples and contain $I$-$V$ characteristics of films with small, medium, and large thicknesses. We find symmetrical curves with a current enhancement of about 2 orders of magnitude as the NC film thickness is increased from 160 to 1073 nm. The log-log graphs in Fig. 2(b) illustrate the nonlinear $I$-$V$ dependence of the data at high voltages. For thin NC films, we typically find a clear transition from a linear to superlinear regime, which can be explained by a space-charge-limited current-transport mechanism [34]. The $I$-$V$ data are fitted using the relation

$$I = aV + bV^m \quad (1)$$

with the parameters $a$, $b$, and $m$ being adjusted to the experimental data [49,50]. For NC films with a large thickness and a mostly linear $I$-$V$ dependence in the measured voltage range, the superlinear part of Eq. (1) is not included in the fit. The parameter $a$ corresponds to the Ohmic conductance $G$ and is used below to estimate the electrical conductivity $\sigma$ of the films. In our data, the power-law coefficient is always in the range $m \approx 2$–3 when its determination is possible. This agrees with the literature, where values of $m = 2$–4 for Si NC films have been reported and indicate that trap states play a major role in the charge transport [27,31,34,51].

To examine the charge-transport properties as a function of the NC film thickness, we fabricate various sets of samples with different thicknesses. In Fig. 3(a), the conductance $G$ is shown as a function of film thickness for three sample sets with different thickness ranges. We find that the conductance increases by about 2.0–2.5 orders of magnitude while increasing the film thickness from $L \approx 100$ to 1000 nm. Above this thickness, the conductance appears to saturate. The conductivity shown in Fig. 3(b) exhibits a similar trend: first, it increases from $10^{-9}\ \Omega^{-1}\,\mathrm{cm}^{-1}$ to $10^{-7}\ \Omega^{-1}\,\mathrm{cm}^{-1}$ with increasing film thickness, and for $L > 1000$ nm, it seems to decrease slightly. This strong variation of the conductivity may

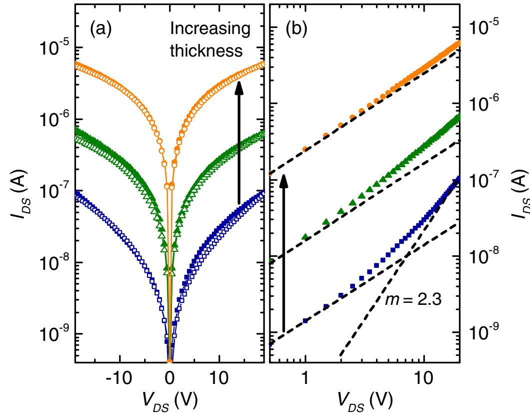


FIG. 2. Drain-source $I$-$V$ characteristics of NC FETs (floating gate) with $L = 160 \pm 60$ nm (blue), $L = 320 \pm 100$ nm (green), and $L = 1073 \pm 190$ nm (orange) in a semilog scale (a) and a log-log scale (b). The filled symbols correspond to measurements with increasing voltage; the open symbols to measurements with decreasing voltage. The dashed lines in (b) symbolize linear and superlinear $I$-$V$ dependences, respectively.

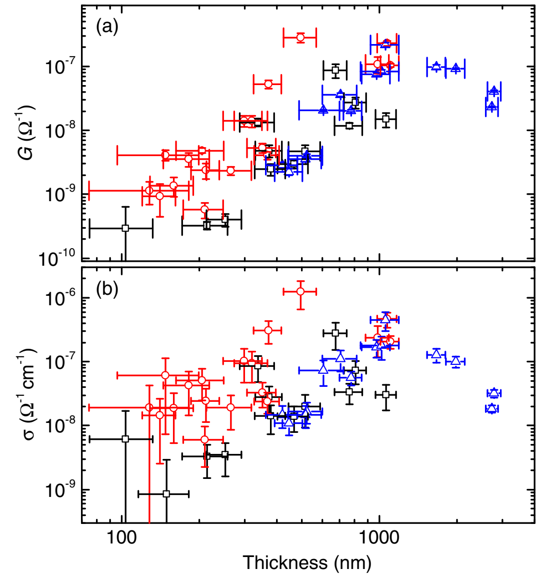


FIG. 3. (a) Conductance $G$ of NC FETs as a function of the film thickness. The data are extracted from fitting $I$-$V$ dependences measured with floating gate, as shown in Fig. 2(b). (b) Conductivity $\sigma$ of the NC FETs calculated from $G$ values given in (a) and the corresponding film thickness, respectively. The different symbols and colors correspond to different sample series.

justify the wide range of conductivities reported in the literature for Si NC films, where conductivities in the range of $10^{-10}$–$10^{-7}$ $\Omega^{-1}\,\mathrm{cm}^{-1}$ are reported [34,35,51]. In our data, the increase of conductance and conductivity is superlinear up to $L = 1000$ nm, with a power-law coefficient around 2.5 and 1.5, respectively. This effect cannot be explained by the geometric increase of the film thickness, which should result in a linear conductance increase and a constant conductivity.

### B. NC FET output characteristics

Figure 4 shows typical transistor-output characteristics for NC FETs in three different thickness ranges. These data are obtained with the same NC FETs used to measure the data shown in Fig. 2. For a thin NC film [Fig. 4(a)], we achieve output characteristics showing a linear dependence for low $V_{\mathrm{DS}}$ and a clear saturation at higher $V_{\mathrm{DS}}$. The NC FETs are working in accumulation mode with electrons as the main charge carriers. When the NC film thickness is increased [Figs. 4(b) and 4(c)], the maximum $I_{\mathrm{DS}}$ increases, and the current at zero and negative gate voltage is enhanced. This effect leads to almost linear output characteristics in Fig. 4(c). Subtracting the output characteristics obtained at $V_G = 0$ V from the data obtained at higher $V_G$, the typical transistor characteristics reappear [Fig. 4(d)]. This shows that the films with large thicknesses still behave in part as transistors but that the layer controlled by the gate voltage is shunted by the remaining film not influenced by the field effect. NC FET output characteristics with shapes similar to Figs. 4(a)–4(c) are reported in the literature [8,9,27–29]; however, the reason for output characteristics without a saturation regime remains unclear [27,28]. We establish here that the NC film thickness plays a major role for this effect, which so far has not been investigated in a consistent and systematic way. In a comparative measurement, we use interdigit structures with different contact spacing in the range of 10 to 160 $\mu$m and films with constant thickness (see the Supplemental Material [46]). We find that the contact spacing does not affect the electrical properties of the Si NC films.

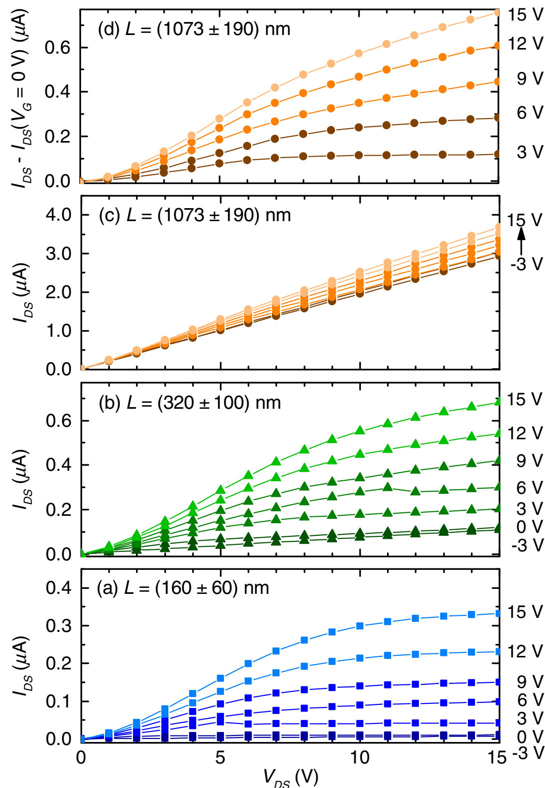


FIG. 4. Output characteristics of NC FETs with (a) $L = 160 \pm 60$ nm, (b) $L = 320 \pm 100$ nm, and (c) $L = 1073 \pm 190$ nm film thickness. (d) shows the data in (c) subtracted by the output characteristic obtained at $V_G = 0$ V. The voltages given on the right axis correspond to the applied $V_G$.

### C. NC FET transfer characteristics

Figures 5(a) and 5(b) show the transfer characteristics of the NC FETs corresponding to the data in Figs. 2 and 4 recorded in the linear regime ($V_{\mathrm{DS}} = 3$ V) and the saturation regime ($V_{\mathrm{DS}} = 13$ V), respectively. For both data sets, $I_{\mathrm{DS}}$ strongly increases above a certain threshold voltage, which is close to 0 V. The $I_{\mathrm{DS}}$ shows a linear increase in the linear regime ($V_{\mathrm{DS}} = 3$ V). In the saturation regime ($V_{\mathrm{DS}} = 13$ V), $\sqrt{I_{\mathrm{DS}}}$ is plotted, which results in a linear behavior above the threshold voltage. We find a hysteresis between the data measured with increasing voltage and decreasing voltage, which indicates charge trapping effects [52]. The hysteresis depends on the applied $V_G$ in the beginning of the measurement and the speed of the voltage sweep, which are both kept constant in all

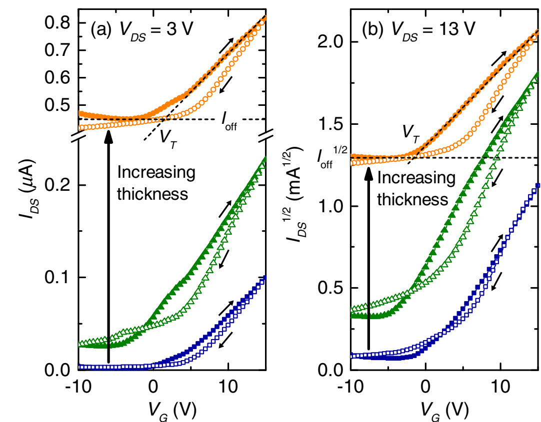


FIG. 5. Transfer characteristics of NC FETs with $L = 160 \pm 60$ nm (blue), $L = 320 \pm 100$ nm (green), and $L = 1073 \pm 190$ nm (orange) film thickness. The filled (open) symbols correspond to a measurement with increasing (decreasing) voltage. The dashed lines represent linear fits to the data, whose intersection with $I_{\mathrm{off}}$ is equal to $V_G$. (a) shows $I_{\mathrm{DS}}$ versus $V_G$ taken at $V_{\mathrm{DS}} = 3$ V; (b) shows $\sqrt{I_{\mathrm{DS}}}$ versus $V_G$ taken at $V_{\mathrm{DS}} = 13$ V.

measurements to ensure consistent data. We further define the minimum value of $I_{\rm DS}$ recorded in the data as the off current $I_{\rm off}$ shown as horizontal dashed lines in Fig. 5. As can be seen already from Fig. 5, $I_{\rm off}$ increases with increasing film thickness, which we further discuss below.

We use the transfer characteristics to calculate the field-effect mobilities $\mu_{\rm lin}$ and $\mu_{\rm sat}$ obtained from the linear and saturation regime data, respectively. Using the gradual channel approximation, we consider for the linear regime

$$(I_{\rm DS} - I_{\rm off}) \cong \frac{WC_i}{S}\mu_{\rm lin}(V_G - V_T)V_{\rm DS}, \tag{2}$$

where $W$ is the transistor channel width, $C_i$ is the specific capacitance per area, $S$ is the electrode spacing, $\mu_{\rm lin}$ is the linear FET mobility, and $V_T$ is the threshold voltage [53]. This equation is valid for small $V_{\rm DS}$ with $V_{\rm DS} \ll (V_G - V_T)$. For high $V_{\rm DS}$ (saturation regime), $I_{\rm DS}$ can be obtained by [53]

$$(I_{\rm DS} - I_{\rm off}) \cong \frac{WC_i}{2S}\mu_{\rm sat}(V_G - V_T)^2. \tag{3}$$

In these experiments, we subtract $I_{\rm off}$ from $I_{\rm DS}$ to account for the finite off current. In Figs. 5(a) and 5(b), two representative examples of the fitting routine are shown (for the filled orange data points). We use Eqs. (2) and (3) to fit the data at voltages above $V_T$, which corresponds to the voltage value of the intersection of the fitted curve with the off current. From these fits, we also obtain the threshold voltage $V_T$ measured from both linear and saturation regime data. A summary of the resulting mobilities and threshold voltages is shown in Fig. 6. Here, the data points are average values of the raw data (all data points) within a thickness range of 100 nm. The linear field-effect mobility scatters around $10^{-5}$ cm$^2$ V$^{-1}$ s$^{-1}$ without a clear dependence on film thickness, and the saturation field-effect mobility ranges between $3 \times 10^{-5}$ cm$^2$ V$^{-1}$ s$^{-1}$ and $6 \times 10^{-6}$ cm$^2$ V$^{-1}$ s$^{-1}$. These values agree well with the literature where field-effect mobilities of $10^{-5}$–$10^{-6}$ cm$^2$ V$^{-1}$ s$^{-1}$ were reported [9,27–29]. The FET channel is expected to be thin (<50 nm) compared to the film thickness of the FETs investigated in this work [28]. Therefore, the mobility of our FETs is not expected to depend on the film thickness, which is in line with our results. The threshold voltages obtained at $V_{\rm DS} = 3$ V and $V_{\rm DS} = 13$ V in Figs. 6(c) and 6(d) scatter around $V_T = 1$–2 V, without any clear thickness dependence. In previous studies, $V_T = 0$–3 V has been estimated for comparable (intrinsic) Si NC FET devices [28]. The threshold voltage can be related to the charge carrier density $n$ using

$$V_T = V_{\rm FB} - \frac{eln}{C_i}, \tag{4}$$

where $V_{\rm FB}$, $e$, $l$ are the flatband potential, the charge of an electron, and the thickness of the FET channel, which is

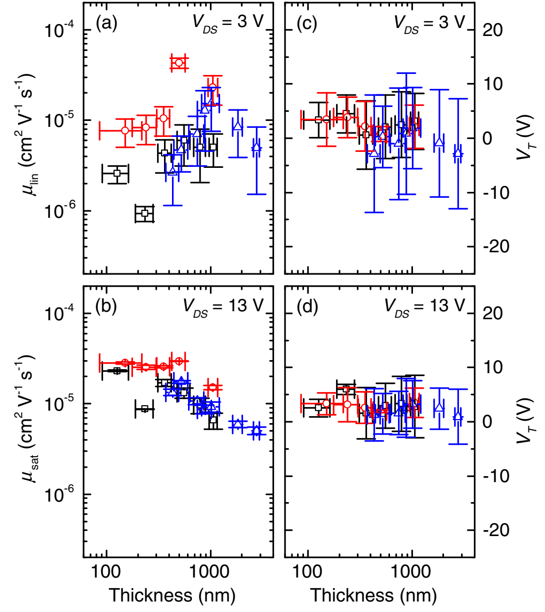


FIG. 6. (a) Linear FET mobility taken at $V_{\rm DS} = 3$ V, (b) saturation FET mobility taken at $V_{\rm DS} = 13$ V, (c) threshold voltage taken at $V_{\rm DS} = 3$ V, (d) threshold voltage taken at $V_{\rm DS} = 13$ V as a function of the NC FET film thickness. All data points are average values of raw data within a thickness range of 100 nm.

estimated to be 50 nm for our accumulation devices [28,53]. According to Eq. (4), a change of $n$ of $10^{17}$ cm$^{-3}$ shifts $V_T$ by $\Delta V_T \approx -1$ V and of $10^{18}$ cm$^{-3}$ by $\Delta V_T \approx -10$ V. In this work, we observe positive threshold voltages suggesting a positive flatband potential, which may be the result of fixed trapped charges [53]. Assuming $V_{\rm FB} = 0 \pm 2$ V, the maximum charge carrier density should not exceed $n \approx 10^{17}$ cm$^{-3}$ for $V_T = 1$–2 V.

## IV. DISCUSSION

### A. Percolation in NC films

In semiconductors with bandlike charge transport, the conductivity $\sigma$ is given by [53]

$$\sigma = e\mu n. \tag{5}$$

In our NC system, we find that $\sigma$ increases by 2 orders of magnitude with increasing film thickness [see Fig. 3(b)]. This increase cannot be explained by a change in mobility, as $\mu$ seems to be constant or has only a very limited variation with thickness [see Figs. 6(a) and 6(b)]. We consider that the charge carrier density $n$ is a material constant and does not depend on the film thickness, which is also reflected in the constant threshold voltage obtained for our NC FETs [see Figs. 6(c) and 6(d)].

In NC systems with hopping charge transport, we propose a modified equation for the conductivity, with the aim to account for the superlinear increase with film thickness observed in our experiments

$$\sigma(L) = e\mu n P(L). \tag{6}$$

Here, $P(L)$ is a percolation factor depending on the film thickness $L$. This percolation factor accounts for a strongly increasing number of hopping possibilities for charge carriers and, thus, charge-transport paths with increasing film thickness. Shklovskii [42] derived

$$P(L) = P_0 \exp\left\{-\xi_c\left[1+\left(\frac{D}{L}\right)^{1/\nu}\right]\right\}, \tag{7}$$

where $P_0$ is a scaling constant, $\xi_c$ is the percolation threshold in the system, $D$ is a characteristic thickness, and $\nu$ is the three-dimensional index of the correlation radius in percolation theory [41,42]. As can be seen in this equation, the number of charge-transport paths increases exponentially for small film thicknesses and saturates when $L \approx D$.

Assuming that the field-effect mobility $\mu$ of the whole film is equal to $\mu_{\mathrm{lin}}$ (or $\mu_{\mathrm{sat}}$), which is measured in the FET channel close to the dielectric-NC film interface, we can compute the experimental values of $nP(L)$ using

$$\frac{\sigma(L)}{e\mu} = nP(L). \tag{8}$$

The results of such a calculation are shown in Fig. 7. We find that $[\sigma(L)/e\mu]$ is enhanced by 2–3 orders of magnitude with increasing film thickness and that for a large film thickness of more than $L \approx 1000$ nm, the values saturate. This behavior confirms that we need the additional term $P(L)$ to describe our experimental data of conductivity $\sigma$, as Eq. (5) alone implies that $(\sigma/e\mu)$ is constant. Using Eq. (7), we define

$$nP(L) = nP_0 \exp\left\{-\xi_c\left[1+\left(\frac{D}{L}\right)^{1/\nu}\right]\right\}$$
$$= A \exp\left\{-\xi_c\left[1+\left(\frac{D}{L}\right)^{1/\nu}\right]\right\}, \tag{9}$$

where $A$ is an adjustable scaling factor. For fitting the data in Fig. 7, all data points in Figs. 7(a) and 7(b) are combined into a single data set. $\xi_c$ is fixed to a mean value of $\xi_c = 0.2$ according to the literature values for bond percolation thresholds of a face-centered cubic lattice ($\xi_c = 0.12$), a body-centered cubic lattice ($\xi_c = 0.18$), and a simple cubic lattice ($\xi_c = 0.25$) [54]. The corresponding fitting curve is shown as dashed lines in Fig. 7. As can be seen, the fit describes reasonably well the data in Figs. 7(a) and 7(b), exhibiting a strong increase at small film thicknesses and starting to saturate around $L = 1000$ nm. From the fit, we obtain $A = 9 \times 10^{16}$ cm$^{-3}$, $D = 3.1 \times 10^3$ nm, and $\nu = 1.08$. $\nu$ is only slightly larger than expected for hopping transport in 3D materials ($\nu = 0.8$–$1$) [40,41,43].

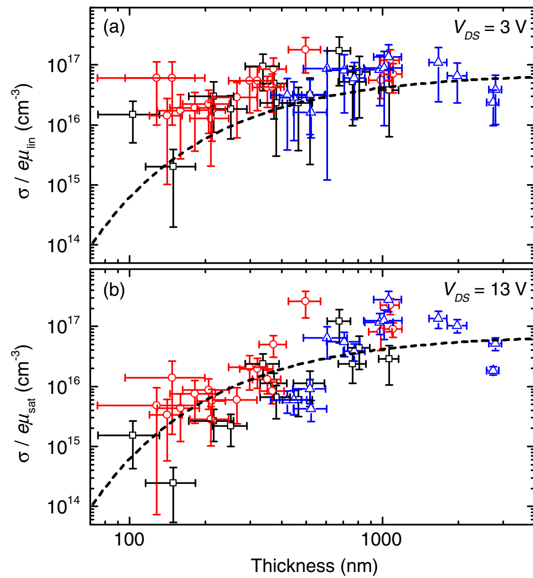


FIG. 7. $\sigma/(e\mu)$ calculated using (a) $e\mu_{\mathrm{lin}}$ and (b) $e\mu_{\mathrm{sat}}$. The dashed line is a fit to all data (a) and (b) using Eq. (9) and $A = 9 \times 10^{16}$ cm$^{-3}$, $\xi_c = 0.2$, $D = 3.1 \times 10^3$, $\nu = 1.08$.

## B. NC field-effect transistor performance

The percolation effects have a strong impact on the performance of the NC FETs. In Figs. 8(g) and 8(h), we show the film-thickness dependence of the ratio between the gated component of $I_{\mathrm{DS}}$ and $I_{\mathrm{off}}$. This ratio $[(I_{\mathrm{on}} - I_{\mathrm{off}})/I_{\mathrm{off}}]$ with $I_{\mathrm{on}} = I_{\mathrm{DS}}(V_G = 15\ \mathrm{V})$ is a measure of the performance of the NC FETs. A high value of $[(I_{\mathrm{on}} - I_{\mathrm{off}})/I_{\mathrm{off}}]$ means that the gated component of $I_{\mathrm{DS}}$ is large compared to $I_{\mathrm{off}}$, and the FETs display the typical output characteristics of a thin-film FET, like that shown in Fig. 4(a). A low value of $[(I_{\mathrm{on}} - I_{\mathrm{off}})/I_{\mathrm{off}}]$ means that $I_{\mathrm{off}}$ is large compared to the gated component of $I_{\mathrm{DS}}$, and the FETs display output characteristics like that shown in Fig. 4(c). The ratio decreases from 200 down to 1 with increasing film thickness, which means that the best-working FETs are obtained for the thinner NC films. To analyze the origin of this behavior, $I_{\mathrm{off}}$ and $I_{\mathrm{on}} - I_{\mathrm{off}}$ are plotted independently in Figs. 8(a)–8(d). The data indicate that the gated component of $I_{\mathrm{DS}}$ is constant, with values of $10^{-7}$ A ($V_{\mathrm{DS}} = 3$ V) and $10^{-6}$ A ($V_{\mathrm{DS}} = 13$ V) independent of the film thickness. This agrees with a FET channel thickness smaller than the thinnest NC FET investigated in our study [28]. As all the film thicknesses in this work are larger than the FET channel thickness, we cannot see a dependence of $I_{\mathrm{on}} - I_{\mathrm{off}}$ on the film thickness. Consequently, the decrease of the NC FETs performance with increasing thickness has to be due to the strong increase of $I_{\mathrm{off}}$, which is shown in Figs. 8(a) and 8(b). The parasitic current $I_{\mathrm{off}}$ increases by 3 orders of magnitude when the film thickness is increased from $L = 100$ nm to $L = 1000$ nm and then saturates at around $10^{-7}$ A for $V_{\mathrm{DS}} = 3$ V and $10^{-6}$ A for $V_{\mathrm{DS}} = 13$ V, respectively. Interestingly, this trend is similar to that

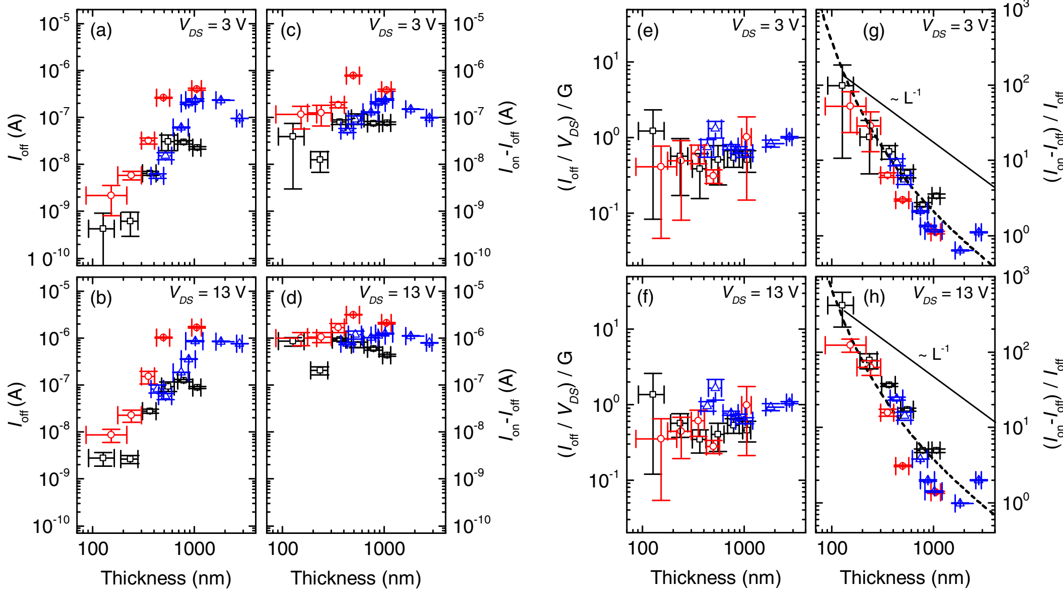


FIG. 8. $I_{\rm off}$ taken at (a) $V_{\rm DS} = 3$ V (b) and $V_{\rm DS} = 13$ V. $I_{\rm on} - I_{\rm off}$ taken at (c) $V_{\rm DS} = 3$ V and (d) $V_{\rm DS} = 13$ V. Ratio of $I_{\rm off}$: $V_{\rm DS}$ to the conductance $G$ taken at (e) $V_{\rm DS} = 3$ V and (f) $V_{\rm DS} = 13$ V. Ratio of $(I_{\rm on} - I_{\rm off})$: $I_{\rm off}$ taken at (g) $V_{\rm DS} = 3$ V and (h) $V_{\rm DS} = 13$ V as well as a fit to the data using Eq. (10) (dashed line). The solid line represents an inverse linear dependence with $L$. Data points in these graphs are average values of the raw data within a thickness range of 100 nm.

observed for the conductance [Fig. 3(a)]. Therefore, we calculate the ratio between $I_{\rm off}$ and $V_{\rm DS}$ (3 V, 13 V) and the conductance. The data are shown in Figs. 8(e) and 8(f). The graphs verify that this ratio does not depend on the film thickness and is similar for the two data sets with values only slightly smaller than 1. This shows that the superlinear increase of $I_{\rm off}$ and the conductance have the same origin. Therefore, our percolation model may also be applied to describe the thickness dependence of $I_{\rm off}$ and the decreasing FET performance with increasing thickness shown in Figs. 8(g) and 8(h). From the definition of the conductivity $\sigma$, it follows $I_{\rm off} \propto \sigma L$, and in Eq. (6) we have described the variation of $\sigma$ with $L$ as $\sigma(L) \propto P(L)$. In this way, we find $I_{\rm off}(L) \propto P(L)L$. Consequently, the FET performance is given by

$$\frac{I_{\rm on} - I_{\rm off}}{I_{\rm off}(L)} = \frac{B}{P(L)L} = \frac{B}{P_0 \exp\{-\xi_c[1 + (\frac{D}{L})^{1/\nu}]\}L} = \frac{K}{\exp\{-\xi_c[1 + (\frac{D}{L})^{1/\nu}]\}L}, \qquad (10)$$

where $B$ is a scaling constant and $K = (B/P_0)$. With Eq. (10), we may describe the data shown in Figs. 8(g) and 8(h). As in the case of the fit shown in Fig. 7 above, we fix the parameter $\xi_c$ to 0.2. The result of the fit is shown as dashed lines in Figs. 8(g) and 8(h). As can be seen, these lines describe the experimental dependence of $[(I_{\rm on} - I_{\rm off})/I_{\rm off}]$ very well. From both fits [Figs. 8(g) and 8(h)], we obtain $D = 2.8 \times 10^3$ nm and $\nu = 1.18$, which are in good agreement with the parameters obtained from the fit of $\sigma/e\mu$ shown in Fig. 7. The scaling constant is $K = 1.1 \times 10^3$ nm [Fig. 8(g)] and $K = 1.9 \times 10^3$ nm [Fig. 8(h)]. Thus, we find that our percolation model is consistent with both sets of data $[(I_{\rm on} - I_{\rm off})/I_{\rm off}]$ and $\sigma/e\mu$, although the experimental values are completely independent.

### C. NC FET charge-transport model

Figure 9 shows a schematic illustration true to scale of our NC FETs. Starting with a thin NC film and applied $V_{\rm DS}$ and positive $V_G$, electrons accumulate close to the interface between the NC film and the dielectric, forming a thin channel (red arrows). At $V_{\rm DS} = 13$ V, the FET is in saturation regime, which means that all the electrons accumulated in the channel contribute to the charge transport from source to drain. As the film thickness increases, more electrons are available that can be accumulated in the channel, and the current in the channel $I_{\rm on} - I_{\rm off}$ is expected to increase. However, we observe a constant $I_{\rm on} - I_{\rm off}$, which suggests that the electric field due to the applied gate voltage is already shielded by the electrons

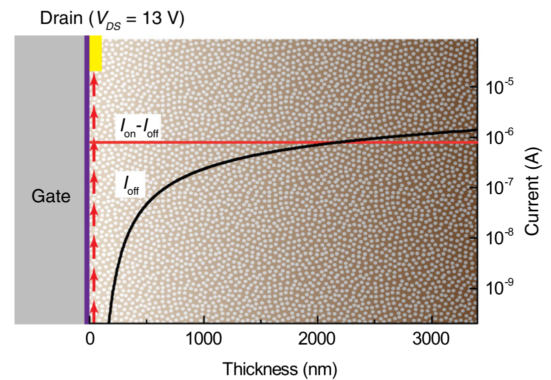


FIG. 9. Schematic illustration true to scale of our NC FETs with an applied voltage of $V_{\rm DS} = 13$ V and a positive $V_G$ applied. The red arrows symbolize the current flowing in the FET channel of $I_{\rm on} - I_{\rm off} = 10^{-6}$ A. $I_{\rm off}$ is depicted from the data in Fig. 8(b).

in a layer that is smaller than 100 nm. Consequently, also the field-effect mobility becomes independent of the film thickness, which agrees with our data (see Fig. 6). In NC films investigated in this study ($L \gg 100$ nm), electrons are transported from source to drain without being affected by $V_G$. This situation is similar to the one with floating gate (see Fig. 3). Therefore, $I_{\mathrm{off}}$ and the conductance show a similar trend [see Figs. 8(e) and 8(f)]. At large film thicknesses around 2000 nm, both the conductance and $I_{\mathrm{off}}$ tend to saturate. We may speculate that although the film thickness is further increasing, the topmost layers are not electrically active.

Importantly, we demonstrate that the strong thickness dependence of the conductance and $I_{\mathrm{off}}$ has a strong impact on the FET performance. We find that the on:off current ratio degrades by 2 orders of magnitude with increasing $L$ [see Figs. 8(g) and 8(h)], which is due to a constant $I_{\mathrm{on}} - I_{\mathrm{off}}$ and a superlinearly increasing $I_{\mathrm{off}}$. This behavior of NC FETs is clearly different from the behavior of conventional FETs based on bulk materials exhibiting bandlike charge transport where a linear dependence of $I_{\mathrm{off}}$ on $L$ is expected and $I_{\mathrm{on}} - I_{\mathrm{off}}$ will be constant. Therefore, the on:off current ratio scales with $1/L$, which is shown as straight lines in Figs. 8(g) and 8(h). As can be seen, this dependence on $L$, neglecting percolation effects, does not describe the data of the NC FETs. We conclude that the increase in film thickness (above the channel thickness) has a much stronger negative impact on the NC FET performance than in the case of conventional FETs. The NC film thickness should be equal to the maximum channel thickness to maximize the transistor performance. We may speculate that our findings can also be applied to other NC-based devices such as photovoltaic cells and light-emitting devices. However, in these applications, the charge carriers are transported along the NC film thickness. This is equivalent to a small electrode spacing and a very large film thickness. Therefore, in these cases, short-channel effects may be dominating and percolation effects should be less relevant.

## V. CONCLUSION

In this work, we investigate the charge transport in NC FETs. We observe that the conductivity of the NC films increases by up to 2 orders of magnitude when the NC film thickness is increased by only 1 order of magnitude, from 100 to 1000 nm. The field-effect mobility is not significantly affected by the changes in film thickness and scatters around $10^{-5}$ cm$^2$ V$^{-1}$ s$^{-1}$. Also, the threshold voltages are quite independent of film thickness. Thus, the increase in conductivity cannot be explained by field-effect mobility changes or a significant change of charge carrier density. Percolation theory is applied to explain the increase of the conductivity as being due to an exponentially increasing number of transport paths present in systems exhibiting hopping charge transport. We show that due to percolation, the NC FET performance dramatically decreases (exponentially) with NC film thickness, which is in contrast to FETs using bulk materials where a weaker (linear) dependence on film thickness is expected. We conclude that the on:off current ratio is dominated by the superlinearly increasing off current as a consequence of percolation effects. Therefore, our work demonstrates that the behavior of NC FETs is much more critically sensitive to variations in film thickness than in the case of conventional FETs based on bulk semiconductors. We anticipate that the performance of NC FETs can be significantly improved further by optimization of NC film thickness.

## ACKNOWLEDGMENTS

The work is supported by the Nano Initiative Munich and by FCT through Project No. PTDC/FIS/112885/2009. TOC image by Nano Initiative Munich.

[1] A. P. Alivisatos, Perspectives on the physical chemistry of semiconductor nanocrystals, J. Phys. Chem. **100**, 13226 (1996).

[2] C. B. Murray, C. R. Kagan, and M. G. Bawendi, Synthesis and characterization of monodisperse nanocrystals and close-packed nanocrystal assemblies, Annu. Rev. Mater. Sci. **30**, 545 (2000).

[3] D. Vanmaekelbergh and P. Liljeroth, Electron-conducting quantum dot solids: Novel materials based on colloidal semiconductor nanocrystals, Chem. Soc. Rev. **34**, 299 (2005).

[4] D. J. Norris, A. L. Efros, and S. C. Erwin, Doped nanocrystals, Science **319**, 1776 (2008).

[5] D. V. Talapin, J.-S. Lee, M. V. Kovalenko, and E. V. Shevchenko, Prospects of colloidal nanocrystals for electronic and optoelectronic applications, Chem. Rev. **110**, 389 (2010).

[6] M. G. Panthani and B. A. Korgel, Nanocrystals for electronics, Annu. Rev. Chem. Biomol. Eng. **3**, 287 (2012).

[7] S. Saeed, C. de Weerd, P. Stallinga, F. C. M. Spoor, A. J. Houtepen, L. Da Siebbeles, and T. Gregorkiewicz, Carrier multiplication in germanium nanocrystals, Light Sci. Appl. **4**, e251 (2015).

[8] M. Härting, J. Zhang, D. R. Gamota, and D. T. Britton, Fully printed silicon field effect transistors, Appl. Phys. Lett. **94**, 193509 (2009).

[9] Z. C. Holman, C.-Y. Liu, and U. R. Kortshagen, Germanium and silicon nanocrystal thin-film field-effect transistors from solution, Nano Lett. **10**, 2661 (2010).

[10] H. Sugimoto, M. Fujii, K. Imakita, S. Hayashi, and K. Akamatsu, Phosphorus and boron codoped colloidal silicon nanocrystals with inorganic atomic ligands, J. Phys. Chem. C **117**, 6807 (2013).

[11] J. M. Luther, M. Law, M. C. Beard, Q. Song, M. O. Reese, R. J. Ellingson, and A. J. Nozik, Schottky solar cells based on colloidal nanocrystal films, Nano Lett. **8**, 3488 (2008).

[12] Q. Dai, C. E. Duty, and M. Z. Hu, Semiconductor-nanocrystals-based white light-emitting diodes, Small **6**, 1577 (2010).

[13] A. H. Ip, S. M. Thon, S. Hoogland, O. Voznyy, D. Zhitomirsky, R. Debnath, L. Levina, L. R. Rollny, G. H. Carey, A. Fischer, K. W. Kemp, I. J. Kramer, Z. Ning, A. J. Labelle, K. W. Chou, A. Amassian, and E. H. Sargent, Hybrid passivated colloidal quantum dot solids, Nat. Nanotechnol. **7**, 577 (2012).

[14] D. K. Kim, Y. Lai, B. T. Diroll, C. B. Murray, and C. R. Kagan, Flexible and low-voltage integrated circuits constructed from high-performance nanocrystal transistors, Nat. Commun. **3**, 1216 (2012).

[15] F. Hetsch, N. Zhao, S. V. Kershaw, and A. L. Rogach, Quantum dot field effect transistors, Mater. Today **16**, 312 (2013).

[16] M. Schnabel, C. Weiss, P. Löper, P. R. Wilshaw, and S. Janz, Self-assembled silicon nanocrystal arrays for photovoltaics, Phys. Status Solidi A **212**, 1649 (2015).

[17] D. L. Klein, R. Roth, A. K. L. Lim, A. P. Alivisatos, and P. L. McEuen, A single-electron transistor made from a cadmium selenide nanocrystal, Nature (London) **389**, 699 (1997).

[18] B. A. Ridley, B. Nivi, and J. M. Jacobson, All-inorganic field effect transistors fabricated by printing, Science **286**, 746 (1999).

[19] D. V. Talapin and C. B. Murray, PbSe nanocrystal solids for *n*- and *p*-channel thin film field-effect transistors, Science **310**, 86 (2005).

[20] M. S. Kang, J. Lee, D. J. Norris, and C. D. Frisbie, High carrier densities achieved at low voltages in ambipolar pbse nanocrystal thin-film transistors, Nano Lett. **9**, 3848 (2009).

[21] M. V. Kovalenko, M. I. Bodnarchuk, and D. V. Talapin, Nanocrystal superlattices with thermally degradable hybrid inorganic-organic capping ligands, J. Am. Chem. Soc. **132**, 15124 (2010).

[22] D. S. Chung, J.-S. Lee, J. Huang, A. Nag, S. Ithurria, and D. V. Talapin, Low voltage, hysteresis free, and high mobility transistors from all-inorganic colloidal nanocrystals, Nano Lett. **12**, 1813 (2012).

[23] S. Z. Bisri, C. Piliego, M. Yarema, W. Heiss, and M. A. Loi, Low driving voltage and high mobility ambipolar field-effect transistors with PbS colloidal nanocrystals, Adv. Mater. **25**, 4309 (2013).

[24] M. I. Nugraha, R. Häusermann, S. Z. Bisri, H. Matsui, M. Sytnyk, W. Heiss, J. Takeya, and M. A. Loi, High mobility and low density of trap states in dual-solid-gated PbS nanocrystal field-effect transistors, Adv. Mater. **27**, 2107 (2015).

[25] S. S. Kim, W.-J. Cho, C.-G. Ahn, K. Im, J.-H. Yang, I.-B. Baek, S. Lee, and K. S. Lim, Fabrication of fin field-effect transistor silicon nanocrystal floating gate memory using photochemical vapor deposition, Appl. Phys. Lett. **88**, 223502 (2006).

[26] X. Zhou, K. Uchida, H. Mizuta, and S. Oda, Carrier transport by field enhanced thermal detrapping in Si nanocrystals thin films, J. Appl. Phys. **105**, 124518 (2009).

[27] S. Weis, R. Körmer, M. P. M. Jank, M. Lemberger, M. Otto, H. Ryssel, W. Peukert, and L. Frey, Conduction mechanisms and environmental sensitivity of solution-processed silicon nanoparticle layers for thin-film transistors, Small **7**, 2853 (2011).

[28] R. Gresback, N. J. Kramer, Y. Ding, T. Chen, U. R. Kortshagen, and T. Nozaki, Controlled doping of silicon nanocrystals investigated by solution-processed field effect transistors, ACS Nano **8**, 5650 (2014).

[29] R. N. Pereira, J. Coutinho, S. Niesar, T. A. Oliveira, W. Aigner, H. Wiggers, M. J. Rayson, P. R. Briddon, M. S. Brandt, and M. Stutzmann, Resonant electronic coupling enabled by small molecules in nanocrystal solids, Nano Lett. **14**, 3817 (2014).

[30] T. A. Burr, A. A. Seraphin, E. Werwa, and K. D. Kolenbrander, Carrier transport in thin films of silicon nanoparticles, Phys. Rev. B **56**, 4818 (1997).

[31] M. A. Rafiq, Y. Tsuchiya, H. Mizuta, S. Oda, Shigeyasu Uno, Z. A. K. Durrani, and W. I. Milne, Charge injection and trapping in silicon nanocrystals, Appl. Phys. Lett. **87**, 182101 (2005).

[32] H. W. Lau, O. K. Tan, and D. A. Trigg, Charge injection and tunneling mechanism of solid state reaction silicon nanocrystal film, Appl. Phys. Lett. **89**, 113119 (2006).

[33] M. A. Rafiq, Z. A. K. Durrani, H. Mizuta, M. M. Hassan, and S. Oda, Field-dependant hopping conduction in silicon nanocrystal films, J. Appl. Phys. **104**, 123710 (2008).

[34] R. N. Pereira, S. Niesar, W. B. You, A. F. da Cunha, N. Erhard, A. R. Stegner, H. Wiggers, M. G. Willinger, M. Stutzmann, and M. S. Brandt, Solution-processed networks of silicon nanocrystals: The role of internanocrystal medium on semiconducting behavior, J. Phys. Chem. C **115**, 20120 (2011).

[35] N. Rastgar, D. J. Rowe, R. J. Anthony, B. A. Merritt, U. R. Kortshagen, and E. S. Aydil, Effects of water adsorption and surface oxidation on the electrical conductivity of silicon nanocrystal films, J. Phys. Chem. C **117**, 4211 (2013).

[36] R. Y. Wang, J. P. Feser, J.-S. Lee, D. V. Talapin, R. Segalman, and A. Majumdar, Enhanced thermopower in PbSe nanocrystal quantum dot superlattices, Nano Lett. **8**, 2283 (2008).

[37] K. Szendrei, Ma. Speirs, W. Gomulya, D. Jarzab, M. Manca, O. V. Mikhnenko, M. Yarema, B. J. Kooi, W. Heiss, and M. A. Loi, Exploring the origin of the temperature-dependent behavior of PbS nanocrystal thin films and solar cells, Adv. Funct. Mater. **22**, 1598 (2012).

[38] C. Grimaldi, Theory of percolation and tunneling regimes in nanogranular metal films, Phys. Rev. B **89**, 214201 (2014).

[39] A. Zabet-Khosousi and A.-A. Dhirani, Charge transport in nanoparticle assemblies, Chem. Rev. **108**, 4072 (2008).

[40] B. I. Shklovskii and A. L. Efros, Percolation theory and conductivity of strongly inhomogeneous media, Sov. Phys. Usp. **18**, 845 (1975).

[41] A. V. Sheinman, Hopping conduction in semiconductor films and critical quantities in percolation theory, Fiz. Tekh. Poluprovodn. **9**, 2146 (1975) [Sov. Phys. Semicond.**9**, 1396 (1976)].

[42] B. I. Shklovskii, Thickness dependence of the hopping conduction in amorphous films. Experiment versus theory, Phys. Status Solidi B **83**, K11 (1977).

[43] K. H. Müller, G. Wei, B. Raguse, and J. Myers, Three-dimensional percolation effect on electrical conductivity in

films of metal nanoparticles linked by organic molecules, Phys. Rev. B **68**, 155407 (2003).

[44] J. Knipping, H. Wiggers, B. Rellinghaus, P. Roth, D. Konjhodzic, and C. Meier, Synthesis of high purity silicon nanoparticles in a low pressure microwave reactor, J. Nanosci. Nanotechnol. **4**, 1039 (2004).

[45] S. Brunauer, P. H. Emmett, and E. Teller, Adsorption of gases in multimolecular layers, J. Am. Chem. Soc. **60**, 309 (1938).

[46] See Supplemental Material at http://link.aps.org/supplemental/10.1103/PhysRevApplied.5.054017 for SEM images and surface profiles of spin-coated Si NC films, FTIR spectra of HF-etched Si NCs, and electrical measurements of Si NC FETs with different FET geometries.

[47] M. Cardona, Vibrational spectra of hydrogen in silicon and germanium, Phys. Status Solidi B **118**, 463 (1983).

[48] V. G. Kravets, C. Meier, D. Konjhodzic, A. Lorke, and H. Wiggers, Infrared properties of silicon nanoparticles, J. Appl. Phys. **97**, 084306 (2005).

[49] A. Rose, Space-charge-limited currents in solids, Phys. Rev. **97**, 1538 (1955).

[50] M. A. Lampert, Simplified theory of space-charge-limited currents in an insulator with traps, Phys. Rev. **103**, 1648 (1956).

[51] L. M. Wheeler, N. R. Neale, T. Chen, and U. R. Kortshagen, Hypervalent surface interactions for colloidal stability and doping of silicon nanocrystals, Nat. Commun. **4**, 2197, (2013).

[52] I. P. Steinke and P. P. Ruden, Percolation model for the threshold voltage of field-effect transistors with nanocrystalline channels, J. Appl. Phys. **111**, 014510 (2012).

[53] S. M. Sze, *Semiconductor Devices, Physics and Technology*, 2nd ed. (John Wiley & Sons, Inc., New York, 2002).

[54] M. B. Isichenko, Percolation, statistical topography, and transport in random media, Rev. Mod. Phys. **64**, 961 (1992).